NEPTUNE_CFD Simulations of DEBORA-Promoteur Experiments: Boiling Freon in a Vertical Pipe with Mixing Vanes

Luc Favre, Stéphane Pujet, Stéphane Mimouni, Catherine Colin

The 19th International Topical Meeting on Nuclear Reactor Thermal Hydraulics (NURETH-19) Log nr.: 19001
Brussels, Belgium, March 6 - 11, 2022

NEPTUNE_CFD SIMULATIONS OF DEBORA-PROMOTEUR EXPERIMENTS : BOILING FREON IN A VERTICAL PIPE WITH MIXING VANES

Luc FAVRE, Stéphane PUJET, and Stéphane MIMOUNI
Mécanique des Fluides, Énergie et Environnement, EDF R&D
6 Quai Watier, 78401 Chatou, FRANCE
luc.favre@edf.fr; stephane.pujet@edf.fr; stephane.mimouni@edf.fr

Catherine COLIN
Institut de Mécanique des Fluides de Toulouse
Université de Toulouse
2 Allée du Professeur Camille Soula, 31400 Toulouse, FRANCE
catherine.colin@toulouse-inp.fr

ABSTRACT

The modeling and simulation of two-phase boiling flows are of primal interest for the nuclear industry since boiling regimes are encountered during Anticipated Operational Occurences (AOO) in Pressurized Water Reactor (PWR) cores. A PWR core is a complex medium including rod bundles, grids and mixing vanes.
In order to investigate the thermal-hydraulics phenomena in such geometries, EDF and CEA conducted a series of experiments on a test facility called DEBORA-Promoteur which consists of a 4m length vertical tube including a mixing device similar to those used in fuel rod bundles. Liquid freon is injected upwards at the inlet and uniformly heated up to boiling. Void fraction is then measured downstream of the mixing device. Experimental flow conditions reach dimensionless numbers representative of PWR. Measurements of the single-phase velocity field and turbulent intensity were also conducted through the AGATE-Promoteur experiment.
In this work, the simulation and modeling of two-phase flows are performed using NEPTUNE_CFD (the eulerian multiphase CFD solver co-developed by EDF, CEA, IRSN and Framatome). Boiling flows in a simple tube are first studied (DEBORA). Then, boiling flow in a tube with mixing vanes is simulated to assess the models' validity on such a geometry (DEBORA-Promoteur). Finally, simulations of single-phase flow through mixing vanes are conducted (AGATE-Promoteur) in order to investigate discrepancies observed in the boiling cases through the liquid velocity field.
This study finally highlights the key governing parameters and variables to improve the modeling of boiling flows in geometries and conditions similar to PWR.

KEYWORDS
boiling flow, mixing vanes, simulation, NEPTUNE_CFD, model analysis

1 INTRODUCTION

Two-phase boiling flows have always been among the most widely studied thermal-hydraulics phenomena in the nuclear industry since boiling in reactors is associated both with enhanced heat transfer and safety issues. Indeed, in Pressurized Water Reactors (PWR), one of the main limiting factors regarding the heat power at the fuel rods' surface in the core is the boiling crisis.

1.1. Boiling crisis in nuclear reactor cores

In a PWR core, the fission exothermal reaction within the fuel rods creates a heat flux which is directly used to heat the water flowing between the rods. During normal operation of the reactor, the water stays in liquid state throughout the whole core. However, during Ancitipated Operational Occurences (AOO), the heat transfer at the rods' surface may be disturbed, leading the water to reach nucleate boiling regime. Even though nucleate boiling is a more efficient way of removing heat from the nuclear fuel, one can not let the heat flux continue to increase since there is a significant risk for the water to evolve from nucleate boiling regime to film boiling regime. The formation of a stable vapor film on a rod's surface creates a local thermal insulation, thus inducing a rapid rise of the rod's temperature which can lead to the rupture of the fuel cladding : this boiling regime transition is called the **boiling crisis**. The heat flux at which this transition occurs is commonly called the **Critical Heat Flux** (CHF).

To avoid water to boil, PWR cores are pressurized up to 155 bar to increase the fluid's saturation temperature. Moreover, fuel rods are hold by grids which role is both to ensure the mechanical stability of the rod bundles and to repel the beginning of nucleate boiling using mixing vanes. Those mixing vanes create a vortex between the rods, enhancing the turbulence of the flow in order to homogenize its temperature along with detaching and condensing potential vapor bubbles which may be created upstream.

1.2. Modeling and simulation of boiling flows in nuclear reactor cores

In order to ensure nuclear reactors' safety regarding the boiling crisis, it is then of primal interest to understand the underlying physics behind thermal-hydraulics phenomena in PWR cores. This explains the extensive research works conducted to model and simulate boiling flows in such medium.

Over the last decades, the tremendous increase of numerical computing capabilities has lead to significant interest and developments in the use of Computational Fluid Dynamics (CFD) to simulate multiphase flows with phase change : **Computational Multi-Fluid Dynamics** (CMFD). Thanks to CMFD, it is now possible to simulate multiphase flows in geometries similar to a nuclear fuel assembly including its grids and mixing vanes. Therefore, numerous research works have proposed simulations of boiling flows in such medium, including single-phase simulations [1, 2], dispersed two-phase boiling flows [3] or CHF predictions [4, 5].

However, such computations require to gather a lot of different models in order to take into account as much physics phenomena as possible (turbulence, wall boiling, coalescence and break-up, condensation, etc.). One of the main difficulty when putting together such a wide range of models concerns their validation and consistency. Models have usually been developed separately and validated against different experimental data, which often do not exactly correspond to industrial flow conditions. This poses an issue to assess the global validity of a code on the aimed complex configurations [6].

In this paper, simulations of both two-phase boiling and single phase flows using NEPTUNE_CFD are presented and analyzed in order to assess models' validity for PWR flows. Section 2 presents the NEPTUNE_CFD code and the associated models. Section 3 is dedicated to simulations of simple tube boiling flow of freon 12 using the DEBORA [7] experimental results. Elements of investigation on the heat flux partition model are also presented. Then, in Section 4, computations of boiling flow of freon 12 in a tube equipped with a mixing device are compared to DEBORA-Promoteur experiments and used to assess the validity of the code on such a geometry. Section 5 presents single-phase flow computations in the same medium (AGATE-Promoteur experiment) and assesses liquid velocity modeling to explain observed dis-

crepancies in the boiling cases. Finally, Section 6 draws conclusions and proposes some ways to improve the modeling of dispersed two-phase flows in PWR conditions.

2 THE NEPTUNE_CFD CODE AND PHYSICAL MODELING

2.1. Simulation framework

NEPTUNE_CFD is an eulerian multiphase CFD solver co-developed by EDF, CEA, IRSN and Framatome mostly for nuclear reactor applications. The code consists of a local three-dimensional modeling based on a two-fluid one pressure approach combined with mass, momentum and energy conservation equations for each phase [8].

The constitutive equations are solved using a pressure correction, based on a finite-volume discretization along with a collocated arrangement of the variables. Moreover, NEPTUNE_CFD allows the use of all type of meshes (hexahedra, tetrahedra, pyramids, etc.), even non-conforming ones, thanks to its face-based data structure. Finally, the code is well-suited for parallel computing, widening its computing capacity to very large meshes.

2.2. Governing equations for turbulent boiling bubbly flows

To simulate two-phase dispersed boiling flows, NEPTUNE_CFD solves the ensemble-averaged equations of mass conservation, momentum balance and energy conservation for each phase (total of 6 equations) :

Mass conservation :

$$\frac{\partial \alpha_k \rho_k}{\partial t} + \overline{\nabla} \cdot \left(\alpha_k \rho_k \overline{U_k} \right) = \Gamma_k \tag{1}$$

Where α_k, ρ_k, $\overline{U_k}$ are the volume fraction, average density and velocity of phase k ; $\Gamma_k = \Gamma_{k,i} + \Gamma_{k,w}$ the interfacial mass transfer term per unit of volume and time splitted between bulk and wall contribution. Subscripts $k = L$ or G denotes the liquid or gas phase, i the interfacial quantities and w the wall contribution.

Momentum balance :

$$\frac{\partial \alpha_k \rho_k \overline{U_k}}{\partial t} + \overline{\overline{\nabla}} \cdot \left(\alpha_k \rho_k \overline{U_k} \otimes \overline{U_k} \right) = -\alpha_k \overline{\nabla} \left(P \right) + \overline{F_{k,i}} + \Gamma_k \overline{U_{k,i}} + \alpha_k \rho_k \overline{g} + \overline{\overline{\nabla}} \cdot \left(\alpha_k \left(\overline{\overline{\tau_{k,m}}} + \overline{\overline{\tau_{k,T}}} \right) \right) \tag{2}$$

Where P is the pressure, $\overline{g}$ the gravity, $\overline{F_{k,i}}$ the interfacial forces accounting for momentum transfer between phases per unit of volume and time, $\overline{U_{k,i}}$ the interfacial velocity, $\overline{\overline{\tau_{k,m}}}$ and $\overline{\overline{\tau_{k,T}}}$ respectively the viscous and turbulent (or Reynolds) stress tensor. Subscript m and T respectively denote the molecular (or laminar) and turbulent terms.

Energy conservation :

$$\begin{aligned}\frac{\partial \alpha_k \rho_k H_k}{\partial t} + \overline{\nabla} \cdot \left(\alpha_k \rho_k H_k \overline{U_k}\right) = &\frac{\partial \alpha_k P}{\partial t} + \Gamma_k H_{k,i} + \overline{F_{k,i}} \cdot \overline{U_k} + Q_{k,i} + \overline{\nabla} \cdot \left(\alpha_k \left(\overline{\overline{\tau_k}} + \overline{\overline{\tau_{k,T}}}\right) \cdot \overline{U_k}\right) \\ &+ \overline{\nabla} \cdot \left(\alpha_k \left(-\left(\lambda_{k,m} + \lambda_{k,T}\right) \overline{\nabla}\left(T_k\right)\right)\right) + \alpha_k \rho_k \overline{g} \cdot \overline{U_k} + Q_{k,w}\end{aligned} \tag{3}$$

Where $H_k = e_k + \frac{U_k^2}{2} + \frac{P}{\rho_k} = h_k + \frac{U_k^2}{2}$ is the total enthalpy of phase k, $H_{k,i}$ the interfacial-averaged enthalpy, $Q_{k,i}$ the interfacial heat flux per unit of volume and time, $\lambda_{k,m}$ and $\lambda_{k,T}$ respectively being the laminar and turbulent thermal conductivity, T_k the temperature, $Q_{k,w}$ the heat flux from the wall to phase k per unit of volume and time.

However, this ensemble-average approach requires a given number of closure laws since this operation removes most of the information about smaller scales physics such as interfacial exchanges between phases or wall-fluid interaction. Terms for which this modeling effort is needed are colored in orange in equations 1, 2 and 3. The chosen expressions for those terms are detailed in subsections 2.3, 2.4 and 2.5.

2.3. Interfacial transfers closure laws

The interfacial transfers of mass, momentum and energy are respectively noted in equations 1, 2 and 3 : Γ_k, $\overline{F_{k,i}}$ and $Q_{k,i}$.

Heat and mass transfers :

The mass transfer terms verify : $\Gamma_{L,i} + \Gamma_{G,i} = 0$, $\Gamma_{L,w} + \Gamma_{G,w} = 0$ with $\Gamma_{G,w} \geq 0$ in the case of boiling flows. This finally gives $\Gamma_L = -\Gamma_G$.

The interfacial heat flux $Q_{k,i}$ can be rewritten in terms of interfacial area concentration a_i : $Q_{k,i} = q''_{k,i} a_i$. Neglecting the mechanical contribution compared to the thermal terms and supposing that the interfacial enthalpy of each phase is equal to its saturation enthalpy, the energy jump condition can then be used to express the bulk condensation rate :

$$\Gamma_{L,i} = \frac{a_i \left(q''_{L,i} + q''_{G,i}\right)}{h_{G,sat} - h_{L,sat}} \tag{4}$$

The interfacial heat flux densities $q''_{k,i}$ and interfacial area concentration a_i are expressed as $q''_{k,i} = C_{k,i}\left(T_{sat}(P) - T_k\right)$ and $a_i = 6\alpha_G / d_G$, d_G being the gas phase Sauter mean bubble diameter. The interfacial area is computed using the transport equation of RUYER & SEILER [9].

For subcooled liquid, the following heat transfer coefficient is used (MANON [10]):

$$C_{L,i} = \frac{Nu_L \lambda_L}{d_G} \text{ and } Nu_L = 2 + 0.6 Re^{1/2} Pr_L^{1/3} \tag{5}$$

Where Re is the bubble Reynolds number $Re = \left|\left|\overline{U_G} - \overline{U_L}\right|\right| d_G / \nu_L$ and Pr_L the liquid Prandtl number $Pr_L = \nu_L / \eta_L$ with ν_L and η_L respectively being the liquid kinematic viscosity and thermal diffusivity.

On the other hand, if the liquid is overheated, the maximum of three heat transfer coefficients accounting for different heat transfer mechanisms (convection heat transfer, stationnary conduction or transient conduction) is taken, following the approach of BERNE [11].

For the gas phase, a simple law that ensures the vapor temperature to remain close to the saturation temperature is used (which is expected for small bubbles, *e.g.* in a PWR) :

$$C_{G,i}a_i = \frac{\alpha_G \rho_v c_{p,G}}{t_c} \tag{6}$$

where $c_{p,G}$ is the gas heat capacity at constant pressure and t_c a characteristic (relaxation) time given by the user (default value being $t_c = 0.01$s) .

Interfacial forces :

The interfacial momentum transfer (excluding the part associated to mass transfer Γ_k) is assumed to be composed of 4 different forces being the drag D, the added mass AM, the lift L and the turbulent dispersion TD :

$$\overline{F_{k,i}} = \overline{F_{k,D}} + \overline{F_{k,AM}} + \overline{F_{k,L}} + \overline{F_{k,TD}} \tag{7}$$

The drag force $\overline{F_{k,D}}$, the added-mass force $\overline{F_{k,AM}}$ and the lift force $\overline{F_{k,L}}$ are respectively expressed following ISHII [12], ZUBER [13] and TOMIYAMA [14]. The turbulent dispersion force $\overline{F_{k,TD}}$ originates from the averaging operation conducted on the three other forces' expressions and is computed as presented in LAVIEVILLE *et al.* [15].

2.4. Turbulence modeling

For bubbly flow simulations, only liquid phase turbulence is taken into account. The prescribed model is the Reynolds Stress Model (RSM) $R_{ij} - \varepsilon\ SSG$ from SPEZIALE, SARKAR and GATSKI [16] adapted to two-phase boiling flows by MIMOUNI *et al.* [17].

2.5. Wall boiling model

The modeling of the heterogeneous boiling phenomenon at the wall is based on a **Heat Flux Partioning** (HFP) model, inspired by KURUL & PODOWSKI original work [18] who divided the wall heat flux density ϕ_w in three terms :

- A single phase convective heat flux $\phi_{c,L}$ heating the liquid through the fraction of the wall area unaffected by the vapor bubbles.
- A vaporization heat flux ϕ_e which accounts for the generation of vapor through wall nucleation.
- A quenching heat flux ϕ_q to represent the thermal impact of bubbles departing from the wall and being replaced by cool liquid.

A fourth flux is added to this HFP in NEPTUNE_CFD, following MIMOUNI *et al.* [19] who consider a convective heat flux heating the vapour $\phi_{c,G}$ when the wall area is covered by a dense accumulation of bubbles.

The model thus gives Equation 8 :

$$\phi_w = \phi_{c,L} + \phi_e + \phi_q + \phi_{c,G} \tag{8}$$

The convective heat fluxes are expressed as $\phi_{c,k} = A_k h_{k,log} \left(T_w - T_k\right)$ with $h_{k,log} = \rho_k c_{p,k} u^* / T_L^+$; where A_k the fraction of the wall area facing phase k, T_w the wall temperature and $h_{k,log}$ the wall logarithmic convective heat transfer coefficient to phase k based on the wall functions for friction velocity u^* and non-dimensional liquid temperature T_L^+ described in 2.6.

The vaporization heat flux is computed following $\phi_e = N_{sit} f \rho_G h_{lg} \pi d_d^2/6$ with :

- N_{sit} the nucleation site density modeled as LEMMERT & CHAWLA [20] : $N_{sit} = \left[210 \left(T_w - T_{sat}\right)\right]^{1.8}$
- f the bubble detachment frequency expressed as COLE [21] : $f = \sqrt{\frac{4}{3}\frac{g|\rho_v - \rho_l|}{\rho_l d_d}}$
- d_d the bubble detachment diameter given by UNAL correlation [22] (Equation 9) :

$$d_d = 2.42\times10^{-5} P^{0.709} \frac{a}{\sqrt{b\varphi}} \text{ with } a = \frac{\left(T_w - T_{sat}\right)\lambda_w}{2\rho_G h_{lg}\sqrt{\pi\eta_w}} \text{ and } b = \begin{cases} \frac{T_{sat}-T_L}{2(1-\rho_G/\rho_L)}, & \text{if } St \leq 0.0065 \\ \frac{1}{2(1-\rho_G/\rho_L)} \frac{\phi_{c,L}+\phi_e+\phi_q}{0.0065\rho_L c_{p,L}\left|\left|\overline{U_L}\right|\right|}, & \text{if } St > 0.0065 \end{cases} \tag{9}$$

where λ_w and η_w are the wall thermal conductivity and diffusivity, $St = \dfrac{\phi_{c,L} + \phi_e + \phi_q}{\rho_L c_{p,L} \left|\left|\overline{U_L}\right|\right| \left(T_{sat} - T_L\right)}$ is the Stanton number and $\varphi = \max\left(1; \left(\dfrac{\left|\left|\overline{U_L}\right|\right|}{U_0}\right)^{0.47}\right)$ with $U_0 = 0.61$m/s.

Finally, the quenching heat flux follows the approach of KURUL & PODOWSKI [18] supposing that it can be modeled as a semi-infinite transient conduction regime : $\phi_q = A_G t_q f \dfrac{2\lambda_L \left(T_w - T_L\right)}{\sqrt{\pi \eta_L t_q}}$ where t_q is the quenching time, supposed to be equal to $1/f$.

2.6. Wall function for dispersed boiling flows

In boiling flows, the formation of bubbles at the wall may disturb the liquid velocity profile in the boundary layer. To take this phenomena into account, MIMOUNI *et al.* [19] proposed a wall function which tends to the single-phase formulation when $\alpha_G \to 0$ and depends on the bubble diameter and density at the wall to add a roughness term in the velocity profile. This approach is the one currently used in NEPTUNE_CFD.

The non-dimensional wall liquid temperature T_L^+ is modeled according to LEDUC [23].

3 BOILING FREON IN A SIMPLE TUBE : DEBORA EXPERIMENTS

In this section, we simulate upward boiling flows of R12 in a vertical tube and compare the NEPTUNE_CFD (NCFD) results with experimental measurements conducted by CEA & EDF on the DEBORA test facility.

3.1. Description of the experiment

In the end of 1990's, CEA and EDF built a test facility called DEBORA which goal was to conduct series of experiments and measurements to establish a database for boiling flows of freon R12. The choice of freon is justified because of its use as a simulating fluid for water in PWR conditions (same phase density ratio, Weber number We, Boiling number Bo and thermodynamic flow quality x_{eq}). Table I sums up the flow conditions scaling between R12 and water.

Table I. Water/R12 scaling (from GARNIER *et al.* [7])

Fluid	Water	Freon R12
Pressure P (bar)	100 - 180	14 - 30
Mass velocity G (kg/m^2/s)	1000 - 5000	1000 - 5000
Wall heat flux ϕ_w (MW/m^2)	0.5 - 6	0.05 - 0.65
Thermodynamic flow quality x_{eq} (-)	(-0.4) - (+0.4)	(-0.4) - (+0.4)

The DEBORA experiment consists of an upward subcooled boiling flow of R12 in a 4m length pipe uniformally heated over 3.5m with an hydraulic diameter $D_h = 19.2$mm. Measurements of void fraction (α), interfacial velocity (*i.e.* axial gas velocity $U_{G,z}$), bubble diameter (d_G), liquid temperature (T_L) and wall temperature (T_w) at the end of the heating length were conducted through different series of tests. Experimental apparatus is detailed in GARNIER *et al.* [7] and MANON [10].

Different test campaigns were conducted on this experimental setup, in particular :

- Campaign 2900 : measurements of α, $U_{g,z}$ and d_G using one optical probe
- Campaign 3000 : measurements of α, $U_{g,z}$ and d_G using two optical probes
- Campaign 800 : measurements of T_L and T_w using thermocouples

Each experimental case is named following this nomenclature : CccGgPppWwwTett with cc being the campaign number, g the inlet mass velocity (G), pp the outlet pressure (P), ww the total heat power applied (W) and tt the inlet temperature (T_{in}). For instance, C8G3P26W23Te69 refers to the case from the campaign 800 with $G \approx 3000$ kg/m^2/s, $P \approx 26$ bar, $W \approx 23$ kW and $T_{in} \approx 69$°C.

3.2. NEPTUNE_CFD simulations of DEBORA cases

In this work, we present the simulations of the following cases :

- C8G2P26W16Te44.9 and C8G2P26W16Te49.6 (single-phase flow)
- C8G2P26W16Te66.6 and C8G2P26W16Te70.3 (two-phase flow)
- C30G2P26W16Te66.6 and C30G2P26W16Te70.6 (two-phase flow)

The pressure of 26 bar is chosen to match the pressure of the mixing vanes cases (DEBORA-Promoteur, Section 4). Mesh sensitivity is performed over two meshes : a large mesh (M1) with 460 356 cells $=$ 338 radial $\times$ 1362 axial cells and a fine mesh (M2) with 3 157 952 cells $=$ 1568 radial $\times$ 2014 axial cells.

On Figure 1, we present the results regarding liquid temperature at the outlet and wall temperature. The liquid temperature profile seems to be correctly reproduced by the simulations, though we see a slight overestimation close to the wall. Looking closer at boiling cases shows a difference of $\approx 0.5°$ C, which is close to the uncertainty of the measurements [7]. Concerning the wall temperature, it appears that it is underestimated before the **Onset of Nucleate Boiling** (ONB) ($T_w < T_{sat}$) and overestimated after the ONB ($\approx +5$°C). Post-ONB wall temperature is characterized by a stabilization of its value above the saturation temperature (here $T_{w,ONB} - T_{sat} \approx 2$°C).

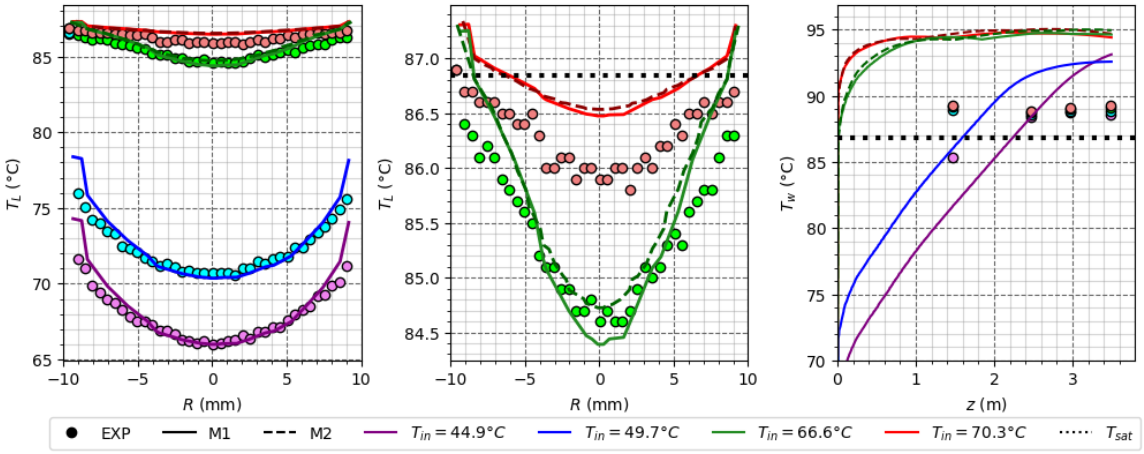

Figure 1. NCFD vs. Exp. - T_L and T_w - Cases C8G2P26W16Te44.9, Te49.6, Te66.6 and Te70.3.

On Figure 2, we compare the results of the simulations to the experiments regarding void fraction, bubble Sauter diameter and axial gas velocity. Void fraction profiles are quite correctly reproduced, though we observe a 10% higher peak at the wall for $T_{in} = 66.6$°C. The order of magnitude of bubble diameter is correct ($\sim$ 0.1mm) and NEPTUNE_CFD manages to detect coalescence (increase of bubble diameter when leaving the wall) and bulk condensation (decrease of bubble diameter when reaching the core of the flow), which is in qualitative agreement with the experiments. Quantitatively speaking, bubble diameter is globally underestimated. Finally, gas velocity profile is reasonably reproduced for $T_{in} = 66.6$°C, but not for $T_{in} = 70.6$°C. The latter experimental profile is flatter, which could be explained by a change of flow regime since uncondensed vapor is detected in the bulk.

Finally, the simulations reasonably agree with the experiments. The strongest discrepancies being mostly the wall temperature and bubble diameter. Potential ways of improving those results are investigated in next sub-section.

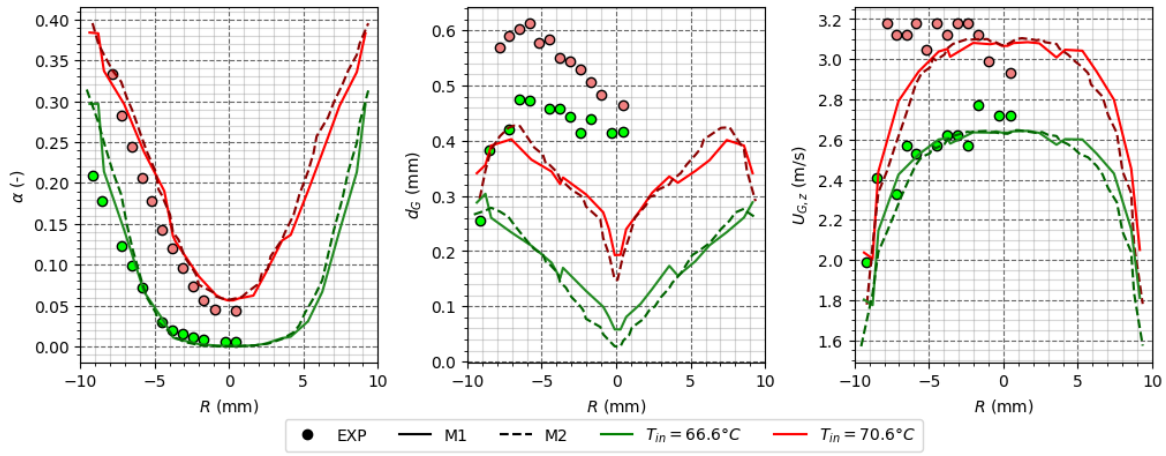

Figure 2. NCFD vs. Exp. - α, d_G and $U_{G,z}$ - Cases C30G2P26W16Te66.6 and Te70.6

3.3. Investigating the nucleation site density modeling N_{sit}

In NEPTUNE_CFD, wall temperature is computed through the Heat Flux Partitioning model, which role is to find the appropriate T_w which balances Equation 8. However, some laws used to express parameters such as N_{sit}, f, or d_d are quite old and simple. For instance, the LEMMERT & CHAWLA [20] expression of N_{sit} only depends on the wall superheat (Sub-section 2.5).

A comparison of the LEMMERT & CHAWLA law [20] with the HIBIKI & ISHII [24] law for N_{sit} against 4 data sets from the literature is presentend on Figure 3. The HIBIKI & ISHII correlation depends simultaneously on wall superheat, pressure and contact angle. Experimental measurements of BORISHANSKII *et al.* [25], RICHENDERFER *et al.* [26], KOSSOLAPOV *et al.* [27] and ZHOU *et al.* [28] are used to assess the two nucleation site density correlations.

Figure 3 clearly shows that the LEMMERT & CHAWLA law lack of pressure dependence fails to reproduce high pressure measurements contrary to the HIBIKI & ISHII one. Even though HIBIKI & ISHII correlation shows significant discrepancies with measurements of KOSSOLAPOV *et al.* and RICHENDERFER *et al.*, its prediction capability is greater in average than LEMMERT & CHAWLA correlation.

To assess the influence of nucleation site density law on NEPTUNE_CFD computations, we compare results obtained with both correlations on Figure 4, which shows a remarkable impact of the modification of N_{sit} correlation. Using HIBIKI & ISHII correlation reduces the error on T_w by approximately 2°C while α and T_L remain unchanged. This implies that the same heat flux partitioning is found with the two models, but that the pressure dependence of HIBIKI & ISHII law helped to balance Equation 8 using a lower T_w, thus closer to experimental measurements.

Such a result indicates that the HFP model could be improved through a systematic analysis of each parameter's impact and modeling (bubble departure diameter, detachment frequency, etc.). Assembling a more recent and consistent model could provide better results regarding wall temperature prediction. Models such as the one developed by KOMMAJOSYULA [29] could be interesting to apply for high-pressure flows.

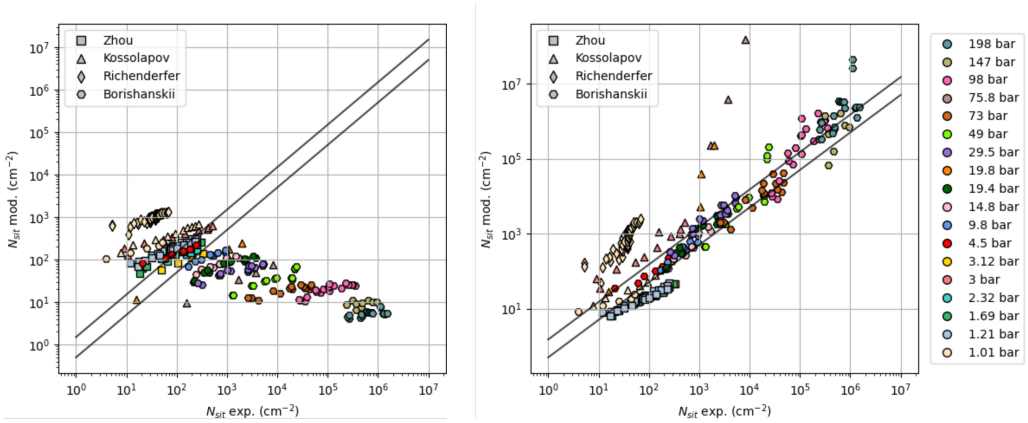

Figure 3. N_{sit} correlations of LEMMERT & CHAWLA (left) and HIBIKI & ISHII (right) vs. exp. data from literature. Operation pressures are displayed. $\pm 50\%$ error bars are drawn in black.

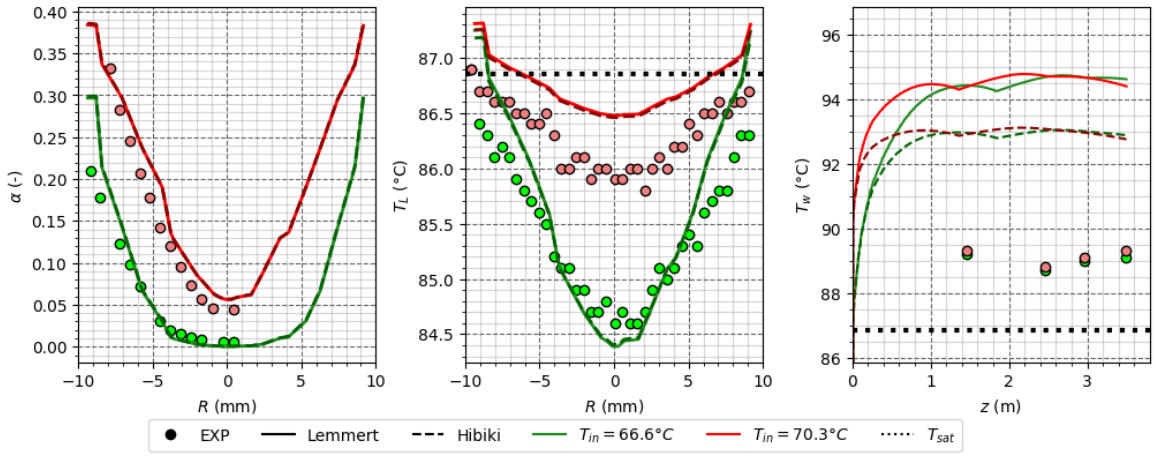

Figure 4. NCFD results for α, T_L and T_w using LEMMERT & CHAWLA and HIBIKI & ISHII correlation. Cases 8G2P26W23Te66.6 and Te70.3, 30G2P26W23Te66.6 and 70.6.

Now that simple tube boiling flow has been assessed through the presented results, next section will focus on the simulation of boiling flow in a tube equipped with a mixing device.

4 BOILING FREON IN A TUBE WITH MIXING VANES : DEBORA-PROMOTEUR EXPERIMENTS

In this section, we simulate upward boiling flows of R12 in a vertical tube equipped with mixing vanes and compare the outlet void fraction profile predicted by NEPTUNE_CFD with measurements coming from the DEBORA-Promoteur experiment.

4.1. Description of the experiment

In 2003, the wish to investigate boiling flows in complex geometries similar to those in PWR fuel assembly lead CEA and EDF to modify the DEBORA facility to introduce mixing vanes (MV) within the tube. This mixing device has been desgined to have the same geometric properties as the mixing vanes attached to rod bundle grids (Figure 5).

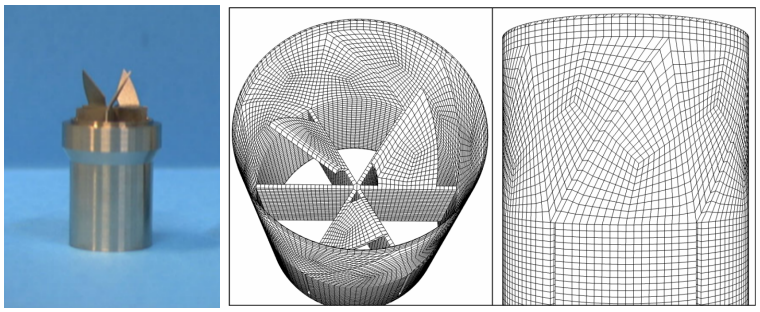

Figure 5. Picture of the mixing device (left) and its fine meshing (right).

Two series of measurements were conducted on this geometry :

- Campaign 4800 : measurements of α using two optical probes, mixing device placed $0.455\text{m} \approx 23.5D_h$ upstream the end of the heating length
- Campaign 5200 : measurements of α and $U_{G,z}$ using two optical probes, mixing device placed $0.192\text{m} \approx 10D_h$ upstream the end of the heating length

The goal of those tests was to observe the impact of the mixing device on the void fraction profile. The induced rotation is expected to gather the bubbles at the center of the tube and enhance condensation for highly subcooled cases. Those expectations are confirmed when looking at experimental α profiles on Figure 6. The strong differences compared to simple tube profiles could explain the gain on the CHF value in PWR thanks to the mixing grids. Cases are named following the same nomenclature as presented in Section 3.

4.2. NEPTUNE_CFD simulations of DEBORA-Promoteur cases

We simulated 3 cases for each position of the mixing device, covering different local thermodynamic quality near the vanes ($x_{eq,MV}$) :

- 48G3P26W23Te65 & 52G3P26W23Te65 with $x_{eq,MV} \approx -1\%$
- 48G3P26W23Te69 & 52G3P26W23Te69 with $x_{eq,MV} \approx 4\%$
- 48G3P26W23Te75 & 52G3P26W23Te75 with $x_{eq,MV} \approx 12\%$

Computations are conducted using two meshes for Te69 cases : a large one (M1) with $444\ 703$ cells and a fine one (M2) with $3\ 487\ 627$ cells. Results for void fraction profiles are shown on Figure 6.

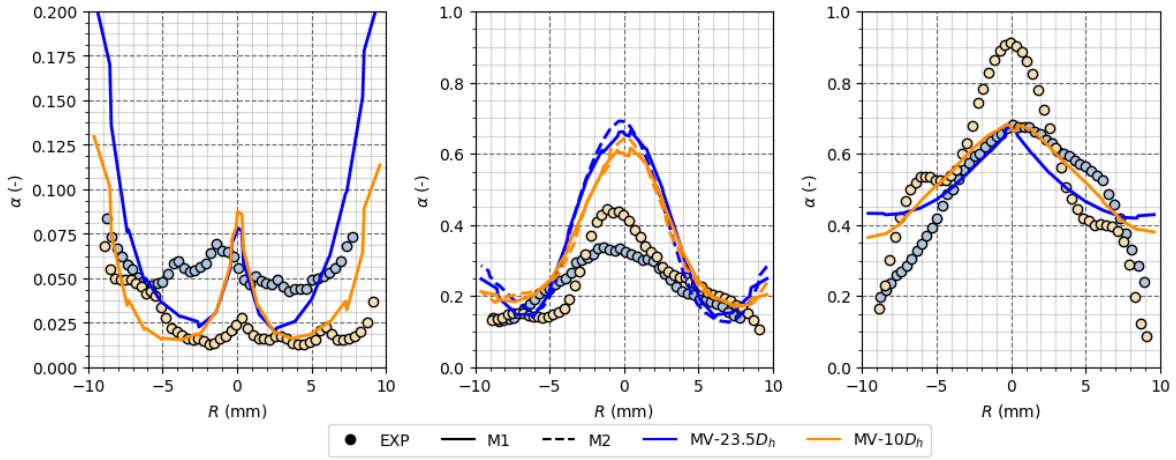

Figure 6. NCFD vs. Exp. - α profiles for two MV positions - $T_{in} = 65°$C (left), $T_{in} = 69°$C (middle), $T_{in} = 75°$C (right).

Quantitatively speaking, it seems that NEPTUNE_CFD reproduces the effect of vapor acculumation at the center thanks to the pressure gradient generated by the swirl induced by the mixing vanes. The radial position of the core void fraction peak correctly matches the experimental one.

However, measured void fraction profiles are not predicted correctly. A particularly strong overestimation of the core void fraction is observed as well as close to the wall. The CMFD results tend to rapidly reach a core void fraction around 60% ($T_{in} = 69°$C cases) and then flattens with increasing temperature ($T_{in} = 75°$ cases). This contradicts experimental observation where the void fraction profile globally rises when inlet temperature increases, except at the wall where no peak is observed due to bubble removing effect by the liquid's rotation. Moreover, the $T_{in} = 75°$ case with MV at $10D_h$ experimentally shows local α peaks at $R \approx \pm 6$mm which remain currently unexplained and not reproduced by the simulations.

To investigate what could be a potential origin for the core void fraction peak overestimation, we present in Section 5 single-phase flow simulations in the MV geometry.

5 LIQUID WATER FLOW IN A TUBE WITH MIXING VANES : AGATE-PROMOTEUR EXPERIMENT

In this penultimate section, we briefly investigate single-phase flow within the same geometry as Section 4.

5.1. Description of the experiment

In 2003, using the same experimental geometry as DEBORA-Promoteur cases (Section 4), Laser Doppler Velocimetry (LDV) measurements of velocity and turbulent fluctutations for an adiabatic single-phase flow of water were conducted. The outlet pressure was around $P = 2$ bar with an inlet mass flux $G \approx 3000$ kg/m^2/s. Measurements were conducted on 6 different diameters and repeated at various axial positions upstream and downstream the mixing vanes.

A first look at experimental measurements (Figure 7) shows that the vanes geometry induces significantly non-symmetric velocity profile. Moreover, we observe high turbulent fluctuations which maximum is located at the same radial position as the maximum radial velocity gradient.

5.2. NEPTUNE_CFD simulations of AGATE-Promoteur case

On Figure 7, we present some of the results obtained with NEPTUNE_CFD using the $R_{ij} - \varepsilon\ SSG$ turbulence model on the M2 mesh, along with a smooth wall law and a rough wall law (roughness $\epsilon = 0.01$mm). The turbulent fluctuations Root Mean Square (RMS) correspond, for instance, to $\sqrt{< u_x'^2 >}$ for the x direction where u_i' represents the fluctuating part of the velocity along compononent i and $< . >$ the time-averaging operator.

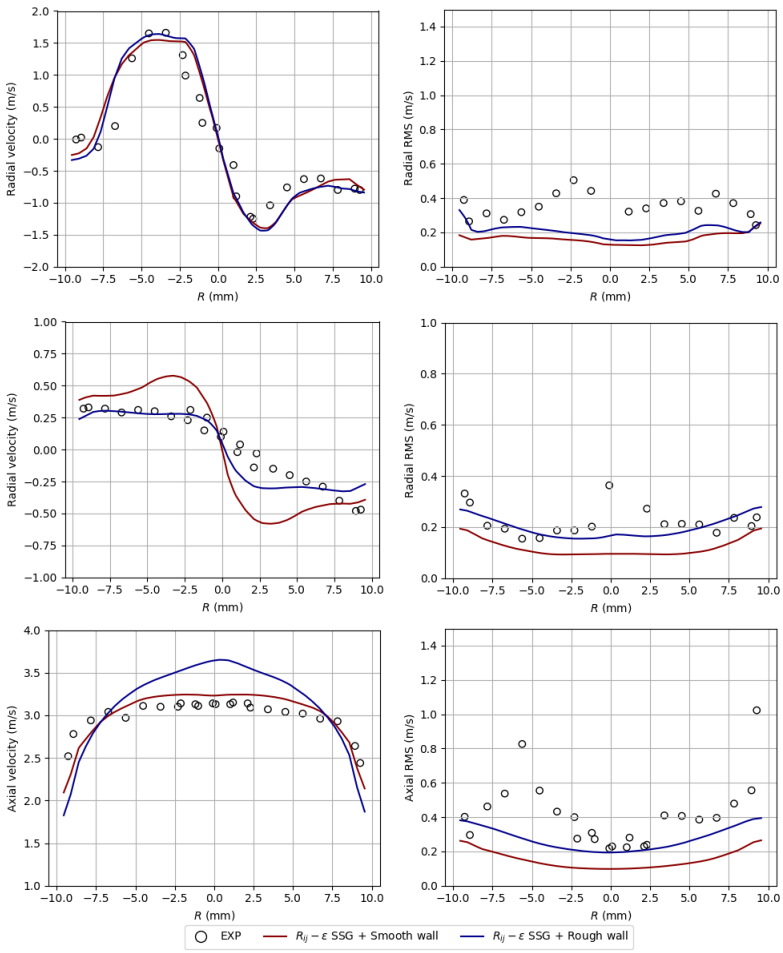

Figure 7. NCFD vs. Exp. - Top & Middle : Radial velocity and turbulent RMS ($z = 30$mm & $z = 440$mm) - Bottom : Axial velocity and turbulent RMS ($z = 440$mm).

Non-symmetric radial velocity profiles close to the MV are quite well reproduced by the simulations. However, far downstream the MV, it appears that the fluid's rotation is overestimated by the model with a smooth wall approach, while applying a roughness helps to reduce the magnitude of the swirl. Moreover, the radial

turbulent fluctuations are better estimated by the rough wall approach at $z = 440$ mm.

On the other hand, it seems that the rough wall approach deteriorates the axial velocity profile compared to the experiment. As shown on the bottom part of Figure 7, the smooth wall simulation returns a flat velocity profile closer to the experiment than the rough wall one which overestimates the core velocity peak.

Both simulations globally underestimate the turbulent fluctuations, which can have a significant influence over the observed discrepancies on velocity profiles since turbulence plays a key role to homogenize the fluid flow.

Those results finally highlight the fact that simulation of such rotating flows may need a particular wall approach to better capture the induced swirl and its dissipation. Correct prediction of turbulent fluctuations would be of significant interest to ensure liquid velocity validation. Further investigations on boiling cases could possibly be improved by a roughness approach, which is the current correction used for two-phase wall laws (Subsection 2.6).

6 CONCLUSION

In this work, we conducted a series of simulations to assess the modeling of boiling two-phase flows both in simple tube and tube with mixing vane geometries.

The simple tube boiling flow cases (Section 3) have shown a reasonable agreement between experiments and simulations with the strongest discrepancies being the wall temperature and bubble diameter. Perspectives to further improve the modeling of such flows are mainly the development of a new Heat Flux Partitioning model, including more recent closure laws for parameters such as nucleation site density or bubble departure diameter.

Then, moving to the tube with mixing vane geometry (Section 4) showed that even though simulations capture core vapor accumulation and condensation, the predicted void fraction profiles strongly differ from experimental measurements. In particular, core and wall void fraction overestimation are observed.

Finally, to investigate boiling flow results in the mixing vane geometry, single-phase flow simulations were conducted (Section 5). The obtained results are of reasonable agreement regarding velocity profiles close to the mixing device, but show an overprediction of the swirl's magnitude downstream the vanes. If applied to a boiling case, this too strong rotation of the fluid could result in an overestimation of the pressure gradient, inducing a rapid migration of the vapor bubbles from the side of the tube towards the center. This could partially explain the very high void fraction peak obtained for boiling cases.

Those observations highlight the fact that ensuring a proper approach to evaluate the Critical Heat Flux for dispersed boiling flows in such geometries needs an extensively validated Heat Flux Partitioning (wall temperature prediction) along with liquid velocity field validation (through liquid turbulence and wall law). This offers promising perspectives for future research works :

- Improving the wall Heat Flux Partitioning through a better modeling of each parameter requiring a closure law (bubble departure diameter, nucleation site density, etc.).
- Detailed investigations of the wall law for both liquid and bubbly flows. Comparison with local

measurements in the boundary layer could be of great interest.

- Assessing the traditionally used turbulence models for those geometries. Such type of work has already been conducted in LEE *et al.* [2] and also found that Reynolds Stress Models may tend to underestimate turbulent fluctuations.
- Collocated experimental measurements of liquid and vapor properties in such rotating flows to provide more recent database in order to assess state-of-the-art CMFD codes.

ACKNOWLEDGMENTS

The authors are grateful to EDF (Électricité de France), CEA (Commissariat à l'Énergie Atomique et aux Énergies Alternatives), IRSN (Institut de Radioprotection et de Sûreté Nucléaire) and Framatome ; those 4 entities contributing to the funding and development of the NEPTUNE_CFD code.

REFERENCES

1. L. Capone, S. Benhamadouche, and Y. A. Hassan, "Source terms modeling for spacer grids with mixing vanes for CFD simulations in nuclear reactors," *Computers and Fluids*, **126**, pp. 141–152 (2016)
2. J. R. Lee, J. Kim, and C. H. Song, "Synthesis of the turbulent mixing in a rod bundle with vaned spacer grids based on the OECD-KAERI CFD benchmark exercise," *Nuclear Engineering and Design*, **279**, pp. 3–18 (2014)
3. T. Cong, R. Zhang, L. Chen, X. Zhang, and T. Yu, "Studies on the subcooled boiling in a fuel assembly with 5 by 5 rods using an improved wall boiling model," *Annals of Nuclear Energy*, **114**, pp. 413–426 (2018)
4. S. J. Kim, "Evaluation of CASL boiling model for DNB performance in full scale 5x5 fuel bundle with spacer grids," Los Alamos International Laboratory (2018)
5. Y. Xu, R. A. Brewster, M. E. Conner, Z. E. Karoutas, and L. D. Smith, "CFD Modeling Development for DNB Prediction of Rod Bundle with Mixing Vanes Under PWR Conditions," *Nuclear Technology*, **205** (1-2), pp. 57–67 (2019)
6. M. Z. Podowski, "Is reactor multiphase thermal-hydraulics a mature field of engineering science?," *Nuclear Engineering and Design*, **345** (January), pp. 196–208 (2019)
7. J. Garnier, É. Manon, and G. Cubizolles, "Local measurements on flow boiling of refrigerant R12 in a vertical tube," in *Multiphase Science and Technology, Vol. 13*, pp. 1–111, (2001)
8. A. Guelfi et al., "NEPTUNE: A new software platform for advanced nuclear thermal hydraulics," *Nuclear Science and Engineering*, **156** (3), pp. 281–324 (2007)
9. P. Ruyer and N. Seiler, "Advanced model for polydispersion in size in boiling flows," *La Houille Blanche*, **4**, pp. 65–71 (2009)
10. E. Manon, *Contribution à l'analyse et à la modélisation locale des écoulements bouillants sous-saturés dans les conditions des Réacteurs à Eau sous Pression*, PhD thesis, Ecole Centrale Paris, 2000
11. P. Berne, *Contribution à la modélisation du taux de production de vapeur par autovaporisation dans les écoulements diphasiques en conduite.*, PhD thesis, Ecole Centrale des Arts et Manufactures, 1983
12. M. Ishii and N. Zuber, "Drag coefficient and relative velocity in bubbly, droplet or particulate flows," *AIChE Journal*, **25** (5), pp. 843–855 (1979)

13. N. Zuber, "On the dispersed two-phase flow in the laminar flow regime," *Chemical Engineering Science*, **19** (11), pp. 897–917 (1964)

14. A. Tomiyama, H. Tamai, I. Zun, and S. Hosokawa, "Transverse migration of single bubbles in simple shear flows," *Chemical Engineering Science*, **57** (11), pp. 1849–1858 (2002)

15. J. Laviéville, N. Mérigoux, M. Guingo, C. Baudry, and S. Mimouni, "A Generalized turbulent dispersion model for bubbly flow numerical simulation in NEPTUNE_CFD," *Nuclear Engineering and Design*, **312**, pp. 284–293 (2017)

16. C. G. Speziale, S. Sarkar, and T. B. Gatski, "Modelling the pressure-strain correlation of turbulence : An invariant dynamical systems approach," *Journal of Fluid Mechanics*, **227** (July), pp. 245–272 (1991)

17. S. Mimouni, J. Laviéville, N. Seiler, and P. Ruyer, "Combined evaluation of second order turbulence model and polydispersion model for two-phase boiling flow and application to fuel assembly analysis," *Nuclear Engineering and Design*, **241** (11), pp. 4523–4536 (2011)

18. N. Kurul and M. Z. Podowski, "Multidimensional Effects in Forces Convection Subcooled Boiling," *Proc. Proceedings of the 9th Heat Transfer Conference*, pp. 21–26, (1990)

19. S. Mimouni et al., "Computational multi-fluid dynamics predictions of critical heat flux in boiling flow," *Nuclear Engineering and Design*, **299**, pp. 28–36 (2016)

20. M. Lemmert and J. M. Chawla, "Influence of flow velocity on surface boiling heat transfer coefficient," in *Heat Transfer in Boiling*, edited by E. Hahne and U. Grigull, pp. 237–247, Academic Press and Hemisphere, New York, (1977)

21. R. Cole, "A Photographic Study of Pool Boiling in the Region of the Critical Heat Flux," *American Institute of Chemical Engineers Journal*, **6** (4), pp. 533–538 (1960)

22. H. C. Unal, "Maximum Bubble Diameter, Maximum Bubble-Growth Time and Bubble-Growth Rate during the Subcooled Nucleate Flow Boiling of Water up to 17.7mn/m2," *International Journal of Heat and Mass Transfer*, **19** (6-E), pp. 643–649 (1976)

23. C. Leduc, *Modélisation de la condensation en film sur les parois d'une enceinte de réacteur*, PhD thesis, Université Joseph Fourier - Grenoble I, 1995

24. T. Hibiki and M. Ishii, "Active nucleation site density in boiling systems," *International Journal of Heat and Mass Transfer*, **46** (14), pp. 2587–2601 (2003)

25. V. Borishanskii, G. Bobrovich, and F. Michenko, "Heat Transfer from a Tube to Water and to Ethanol in Nucleate Pool Boiling," in *Problems of Heat Transfer and Hydraulics of Two-Phase Media*, edited by S. S. Kutateladze, pp. 85–106, Pergamon Press, Moscow, (1969)

26. A. Richenderfer et al., "Investigation of subcooled flow boiling and CHF using high-resolution diagnostics," *Experimental Thermal and Fluid Science*, **99**, pp. 35–58 (2018)

27. A. Kossolapov, B. A. Philipps, and M. Bucci, "Experimental investigation of bubble dynamics in subcooled flow boiling of water at prototypical pressure of boiling water reactors," *Proc. CFD for Nuclear Reactor Safety Applications (CFD4NRS-8) - Workshop Proceedings*, (2020)

28. P. Zhou, R. Huang, S. Huang, Y. Zhang, and X. Rao, "Experimental investigation on active nucleation site density and bubble departure frequency in subcooled flow boiling by using bubble tracking algorithm," *International Journal of Heat and Mass Transfer*, **148** (2020)

29. R. Kommajosyula, *Development and assessment of a physics-based model for subcooled flow boiling with application to CFD*, PhD thesis, Massachusetts Institute of Technology, 2020